12^{th} International Conference on Fracture Mechanics of Concrete and Concrete Structures
FraMCoS-12
B.L.A. Pichler, Ch. Hellmich, P. Preinstorfer (Eds)

https://doi.org/10.21012/FC12.1122
TT-B:1

DIRECT TENSION TEST ON LARGE CONCRETE SPECIMEN: MONOTONIC VERSUS FATIGUE LOADING

YOGESH R[*1], KAMAL ANAND[*2], and J. M. CHANDRA KISHEN[*3]

[*] Department of Civil Engineering, Indian Institute of Science
Indian Institute of Science
Bangalore, 560012, India
[1] e-mail: yogeshr@iisc.ac.in
[2] e-mail: kamalanand@iisc.ac.in
[3] e-mail: chandrak@iisc.ac.in

Key words: Concrete, Crack mouth opening displacement, Direct tension, Fracture process zone, Fatigue, Micromechanics

Abstract. The tensile strength of concrete plays a vital role in the design of large concrete infrastructures. Further, the majority of these structures are subjected to cyclic loading, causing fatigue. Most of the properties under monotonic and fatigue loadings are obtained from tests conducted on small-sized specimens. Since concrete exhibits a strong size effect due to its heterogeneous nature, it is imperative to determine the properties of large specimens. This study aims to conduct a stable, direct tension test on 400 x 400 x 100 mm sized concrete prismatic specimens to investigate the differences in fracture mechanism under both monotonic and fatigue loading. The acoustic emission (AE) and digital imaging are used to capture the evolution of microcracking during the monotonic and fatigue tests. It is observed that the tensile strength of concrete is about 4-5% of the characteristic compressive strength, which is nearly half of the value considered in the literature. Further, the mechanism of microcracking is significantly different under monotonic and fatigue loadings.

1 Introduction

Concrete is the commonly adopted material in construction and is extensively used to build various structures such as high-rise buildings, dams, tunnels, and bridges. The behavior of concrete has been thoroughly studied over the decades, and these studies are utilized to design structures by adhering to various limit states of serviceability and strength. Ensuring that a structure meets these criteria is essential for its safe design. In the design of large structures, including dams and nuclear power plants, it is assumed that the tensile strength (f_t) of concrete is zero [1]. This is despite the fact that literature and various codal standards report the tensile strength as being 8-15% of its compressive strength (f_{ck}) after 28 days of wet curing. Typically, the fundamental elastic properties of concrete are evaluated using small cubes of size 150 mm and cylindrical specimens with a height of 300 mm and diameter of 150 mm. However, real structures are much larger, and concrete exhibits strong size effects due to its heterogeneous nature [1].

Cracking is an inherent feature of any cementitious material, including concrete. However, these develop into structural cracks when the applied stress exceeds the tensile strength, leading to visible and more complex cracks. To enhance the safety and reliability of concrete structures, it is crucial to incorporate a comprehensive understanding of fracture mechanics and size effects into design practices [2, 3]. This approach can help to mitigate the risks associated with overloading and other factors that contribute to structural failures.

Fracture-based design necessitates a thorough understanding of the fracture behavior of concrete under tension. Current design philosophies predominantly rely on indirect tension tests, such as three-point or four-point bending tests (flexural tests) on beams, splitting tension (Brazilian) tests on cylinders, and wedge-splitting tests on compact tension specimens [4–6]. Mier and Vliet [7] have stated the importance of determining the fracture properties of concrete and similar disordered materials (rock, clay, ice, bricks, etc.) using the uniaxial tension test. However, direct tension tests are less frequently discussed in the literature [8–10]. Some direct tension tests are conducted on small-sized specimens, including cylinders, rectangular prisms [11], and dog bone-shaped specimens. This is primarily due to the numerous challenges encountered in conducting the direct tension tests [12, 13]. Major difficulties include [1]:

- Ensuring proper alignment without causing eccentricities during the cracking process.
- Securing the specimen with proper fixtures.
- Maintaining the stability of the specimen geometry.
- Using testing equipment capable of stable experimental control.
- Significant time required for these tests.
- Additionally, there are no standardized protocols for performing these types of experiments on a large-scale.

The above challenges are overcome in this research by creating a bi-axial test facility (as explained later on) wherein large-size specimens can be tested in displacement control under monotonic and load control fatigue loading. This facility is supplemented by acoustic emission and digital imaging monitoring systems to study the mechanisms of micro-crack nucleation and its growth. This will provide more insights into concrete fracture and failure behavior that have not been seen in previous studies.

Many concrete structures are subjected to repetitive loading, and failure in such conditions occurs due to fatigue. Under fatigue, the accumulation of internal microstructural damages occurs even under lower amplitudes of loading. Reinhardt and his research group [1,14,15] have conducted cyclic loading tests on prismatic specimens using tension-compression loading. Many other researchers have conducted fatigue tests of concrete under tension using cylindrical specimens. However, to the best of authors knowledge, fatigue tests on large concrete specimens under direct tension are not reported in the literature [16].

In this work, large-sized double-edge notched prismatic concrete specimens are prepared and tested under monotonic and fatigue loading. The main objective is to identify the differences in the mechanisms of crack growth under these two types of loading. This is achieved through the tracking of the micro-cracking process using acoustic emission and digital imaging techniques.

2 Materials and preparation of specimens

This section contains the details of the materials used in the preparation of the direct tension specimens.

Plain concrete prismatic specimens were prepared as per the mix design protocol given in the Indian Standard Code IS 10262-2016 [17]. The mix of concrete contains Ordinary Portland Cement (OPC) of grade 53, river sand which passes through a 4.75 mm sieve, and graded coarse aggregates of crushed granite stone having a maximum size of 12.50 mm.

The water-to-cement ratio (w/c) is taken as

0.50, and the mix ratio of cement:fine aggregate:coarse aggregate is 1:2.30:2.70. Based on this mix ratio, direct tension specimens are prepared together with cubes (150 mm) and cylinders (diameter (ϕ)-150 mm, and height 300 mm) for evaluating the elastic properties of the material.

Figure 1 shows the geometric details of the specimens used in the experiment. The direct tension specimens are prismatic, with a length of 400 mm, height of 400 mm, and thickness of 100 mm. The prismatic specimens are provided with notches of 2 mm width and length of 100 mm provided at mid-height at both ends (notch-to-depth ratio (a/D) 0.25), thereby creating a double-edge notched specimen. These specimens were fixed with two steel plates of 30 mm thickness while casting itself using nine numbers of 16 mm diameter rebars. The steel plates had threaded holes for fixing the specimen to the platens of the testing machine using bolts. The freshly prepared concrete was poured into steel forms, which were placed with their large faces horizontally down. The 30 mm steel plates welded with steel rebars were kept inside the forms in position, and the concrete mix was poured and vibrated.

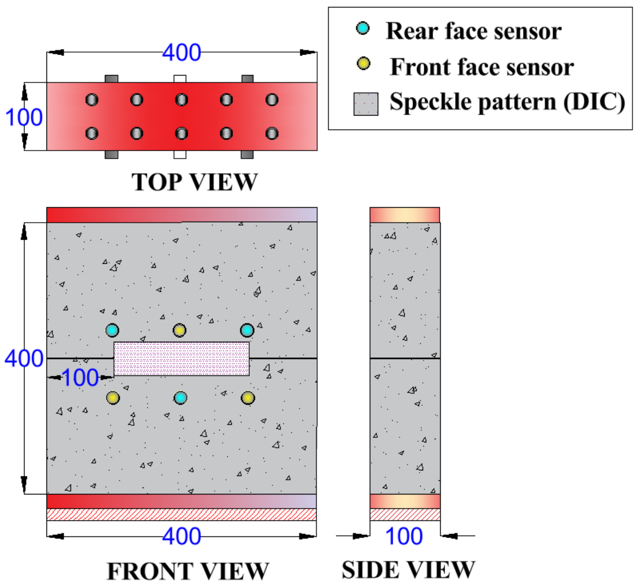

Figure 1: Geometrical details of the specimen

All specimens were removed from the molds after a day and cured in water for 28 days. The cubes and cylinders are tested using standard procedures, and their elastic properties are determined. The mean and standard deviation (SD) of elastic properties are shown in Table 1.

Table 1: Details of elastic properties (cubes and cylinders)

Properties (in MPa)	**Mean**	**SD**
Compressive strength, f_{ck}	48.00	3.45
Splitting tensile strength, f_{sp}	3.36	0.21
Modulus of elasticity, E	34205	2155

3 Test setup and experimental procedure

The direct tension tests were conducted on a large stiffness biaxial setup manufactured by M/s ITW India. The biaxial setup is a servo-hydraulic system consisting of four orthogonally placed independent actuators with 500 kN capacity each. The specimen was placed vertically and fixed to the vertical actuator, which measures the load and deflection through the in-built load cells and strain gauges. The special feature of this machine is its capability to apply uniaxial tensile loading without creating any eccentricities during the cracking process. This is possible through the linear variable differential transducers (LVDT) provided on each actuator that senses the eccentricities and applies displacements to counter this effect. Figure 2 shows the machine with the specimen attached to the vertical actuators. Figure 3 illustrates the notch dimensions and the location of the clip gauge to control and measure the crack opening, which is attached near the notch mouth. The specimen was instrumented with six acoustic emission (AE) piezoelectric sensors, of which three are mounted on the front and three on the back face of the specimen. These AE sensors capture the micro-cracking activity that takes place inside the specimens. While the AE data provides micro-cracking information inside the specimen, simultaneous digital imaging captures the displacement and strain profiles on the specimen faces. For this imaging, a speckle pattern is created on the specimen face in the region between the notches spanning 50 mm in height and 200 mm in length using black spray paint. A camera was mounted in front of the specimen that captured the images at regular intervals as the experiment progressed. These images were analyzed using built-in correlation algorithms in imaging post-processing software to determine surface displacements and strains.

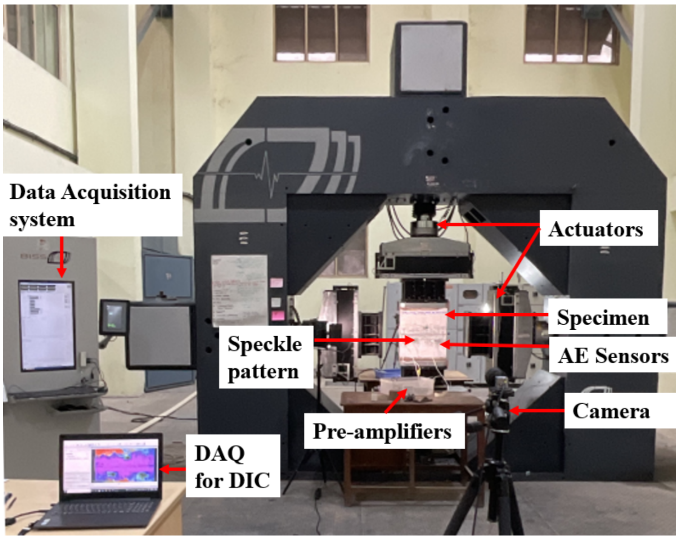

Figure 2: Experimental setup

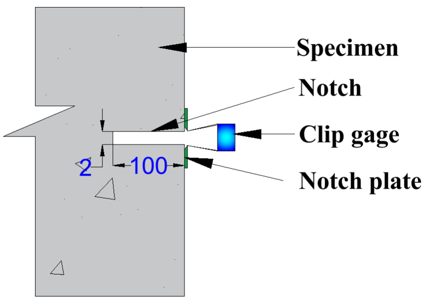

Figure 3: Details of notch and positioning of CMOD

The specimens are tested using two different loading protocols - monotonically increasing crack mouth opening displacement (CMOD) and cyclic fatigue loading. In the monotonic tests, the loading is done using CMOD control in order to obtain the complete post-peak response. Here, the clip gauge is used to control the test with the rate of crack opening set to 0.0001 mm/s.

In the fatigue tests, harmonic tensile cyclic loading is applied to the specimens with constant amplitude and variable frequency. The maximum amplitude (P_{max}) was set to 19.40 kN, which is 50% of the average peak load in the monotonic test, and the minimum load (P_{min}) was set to 7.76 kN, which corresponds to 20% of mean peak-load of the monotonic test. The stress ratio (R), which is the ratio of minimum to maximum load $\left(R = \frac{P_{min}}{P_{max}}\right)$, is 0.40 in the tension region. The frequency of applied loading was kept small in the beginning and gradually increased as the test progressed. This was done to prevent sudden failure of the specimen. The minimum frequency of the fatigue loading was 0.01 Hz while the maximum was 0.5 Hz. The magnitude and frequencies of the cyclic test are shown in Figure 4.

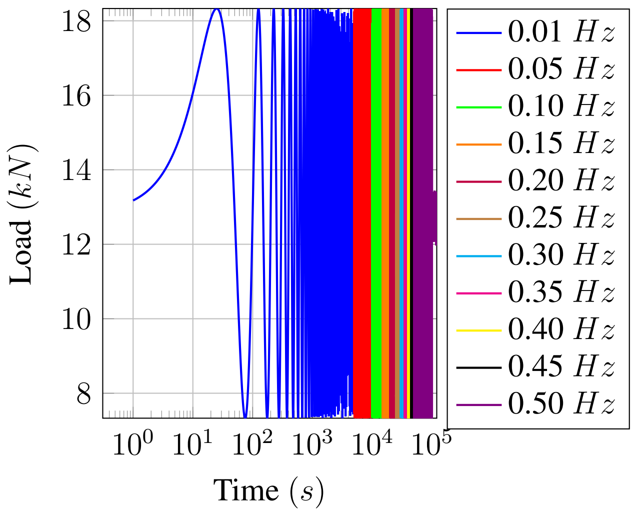

Figure 4: Loading details of the fatigue test

4 Results and discussion

The various observations and results from the monotonic and fatigue experiments are explained in this section.

4.1 Behavior under monotonic loading

Three notched prismatic specimens were tested under monotonically increasing crack mouth opening displacement at a rate of 0.0001

mm/s in a servo-hydraulic testing machine under direct tension. As mentioned earlier, the stiff testing machine can negate any eccentricities that are caused during the cracking process, thereby ensuring a proper alignment under pure tension. Figure 5 shows the load versus CMOD curves of the three specimens. From these curves, it is seen that the material behaves linear elastically until 75-80% of the peak load in the initial pre-peak region. The slope of the linear elastic portion, termed the initial stiffness, was computed for the three specimens, and the average value obtained was 1562.03 kN/mm. However, beyond this linear portion, the specimens show nonlinear behavior up to peak load. The average peak load measured from the vertical actuator was 38.80 kN, and the corresponding average value of CMOD noted from the clip gauge was 0.040 mm, respectively.

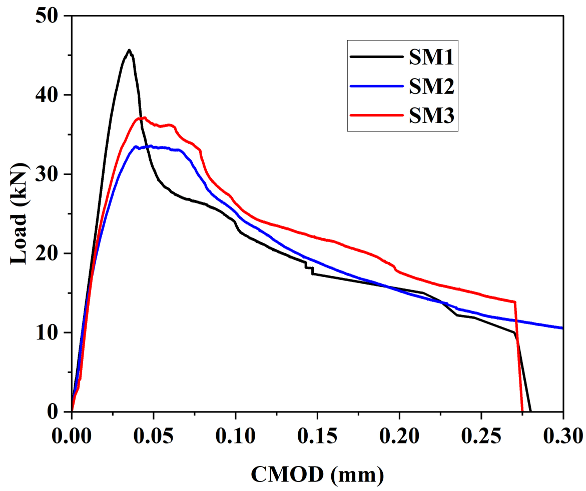

Figure 5: Load versus CMOD curves

Table 2: Fracture properties from monotonic tests

Specimen number ⇓	Initial slope	Peak load	CMOD peak	CMOD failure	Area load-CMOD	Fracture energy	Tensile strength
	N/m	kN	mm	mm	Nm	N/m	MPa
1	1562.03	45.67	0.032	0.275	5.57	278.62	2.28
2	1274.54	33.58	0.044	0.312	5.62	280.88	1.68
3	1781.48	37.15	0.044	0.280	6.21	310.62	1.86
Mean	1562.03	38.80	0.040	0.289	5.80	290.08	1.94
Standard deviation	234.74	5.07	0.006	0.016	0.28	14.58	0.25

The tensile strength is a material parameter, which is calculated as the ratio of peak load to uncracked ligament area (200 × 100 mm). The average tensile strength yielded a value of 1.94 MPa. The average compressive strength of a cube having size 150 x 150 x 150 mm was determined to be 48 MPa. The ratio of tensile strength to compressive strength works out to be 4.04%. The relationship between tensile (f_t) and compressive strength (f_{ck}) can be written in the form

$$f_t = \alpha\sqrt{f_{ck}} \tag{1}$$

Where α is the coefficient, which is estimated as 0.28. Equation 1 can be rewritten as $f_t = 0.28\sqrt{f_{ck}}$. The corresponding equation, as suggested by the Indian Standard code IS 456-2000 [18], is $f_t = 0.7\sqrt{f_{ck}}$ for flexural tension case. The flexural tensile strength is seen to be much higher than the measured value under the direct tension of a large concrete specimen. Table 2 gives the fracture properties obtained under monotonic testing of large concrete specimens under direct tension.

4.2 Behavior under fatigue loading

Conducting a fatigue test under direct tension on concrete specimens is quite challenging since a small eccentricity or an overload or a large frequency of loading can break the specimen. Hence, a loading protocol with frequency varying from an initial small value to higher values was defined as shown in Figure 4. As seen in this figure, steps 1 and 2, with 50 cycles each, have a frequency of 0.01 and 0.05 Hz, respectively. Steps 3-10 have 5000 cycles each, and in each step, the frequency increases by 0.05 Hz. The last step is designed for 100,000 cycles of 0.5 Hz frequency.

Figure 6 shows the plot of maximum CMOD, which is the CMOD corresponding to the maximum load in every loading cycle as a function of the number of loading cycles. There is a gradual increase in the CMOD with increasing fatigue loading cycles. Figure 7 shows the degradation in stiffness with an increasing number of fatigue loading cycles. Here, the stiffness is gradually reduced with increasing loading cycles. The gradual increase in the CMOD and the decrease in stiffness is a consequence of the evolution of micro-cracks and their coalescence during fatigue loading. The mechanisms of the crack growth taking place during the fatigue process are well captured and explained later on from the results of the acoustic emission.

Table 3: Features from fatigue experiments

Step	Number of cycles	Frequency	Max. CMOD Initial	Max. CMOD Final	Stiffness Initial	Stiffness Final
$\Downarrow$	**Units** $\Rightarrow$	Hz	mm	mm	kN/mm	kN/mm
1	50	0.01	0.00328	0.00409	3328.89	3226.79
2	50	0.05	0.00411	0.00418	3260.50	3261.60
3	5000	0.10	0.00417	0.00528	3276.30	3124.80
4	5000	0.15	0.00524	0.00590	3122.80	3115.60
5	5000	0.20	0.00580	0.00580	3113.30	3113.80
6	5000	0.25	0.00574	0.00585	3110.70	3124.70
7	5000	0.30	0.00582	0.00592	3113.50	3112.20
8	5000	0.35	0.00586	0.00589	313.80	3112.80
9	5000	0.40	0.00573	0.00598	3127.77	3101.14
10	5000	0.45	0.00590	0.00630	3096.50	3109.40
11	100000	0.50	0.00630	0.0650	3103.83	3064.34

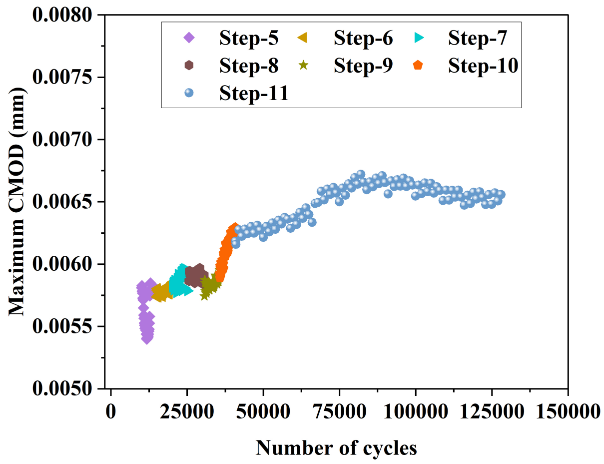

Figure 6: CMOD with number of cycles

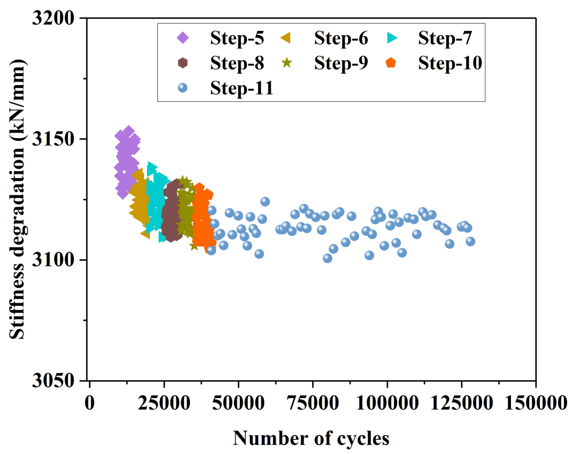

Figure 7: Stiffness degradation with number of cycles

Table 3 shows the variations in the maximum CMOD and stiffness at different steps of fatigue loading.

4.3 Results from acoustic emission data analysis - Differences in the behavior under monotonic and fatigue loading

In this section, the fracture mechanisms for the failure of concrete in direct tension under monotonic and fatigue loading are analyzed and discussed using the data from the distribution of acoustic emission events and energy.

Figure 8 shows the distributions of acoustic emission (AE) events at different loading stages of the load-CMOD curve of specimen number three. No events were observed up to 50% of load in the pre-peak region. The AE events started appearing at about 70-80% of pre-peak loading, indicating the beginning of micro-cracks formation. A few events had occurred at peak load close to the right notch tip. This indicates the localization of fracture taking place at one of the notch tips. As the monotonically increasing CMOD progresses, leading to the softening behavior (as seen in Figure 5), the number of AE events is seen to increase, moving towards the left notch tip. This increase in AE events indicates the growth of micro-cracks in a localized region of the right notch tip, known as the fracture process zone. Many toughening mechanisms, including crack shielding and crack branching, besides others, occur in the fracture process zone. Final failure occurs when this zone of micro-cracks approaches the left notch tip.

In contrast, the occurrence of AE events or the micro-cracks under fatigue loading shows a completely different picture. Hardly any events are seen for a major portion of the fatigue life. The events begin to appear only in the last stage of fatigue, just before final failure. Figure 9 shows the distribution of AE events that are formed in the last few cycles of the fatigue loading. Only about twenty AE events are formed, with the majority forming in the last few cycles. Furthermore, the AE events are distributed in the uncracked ligament between the two notch tips. There is no localization of fracture, as seen in the case of monotonic loading.

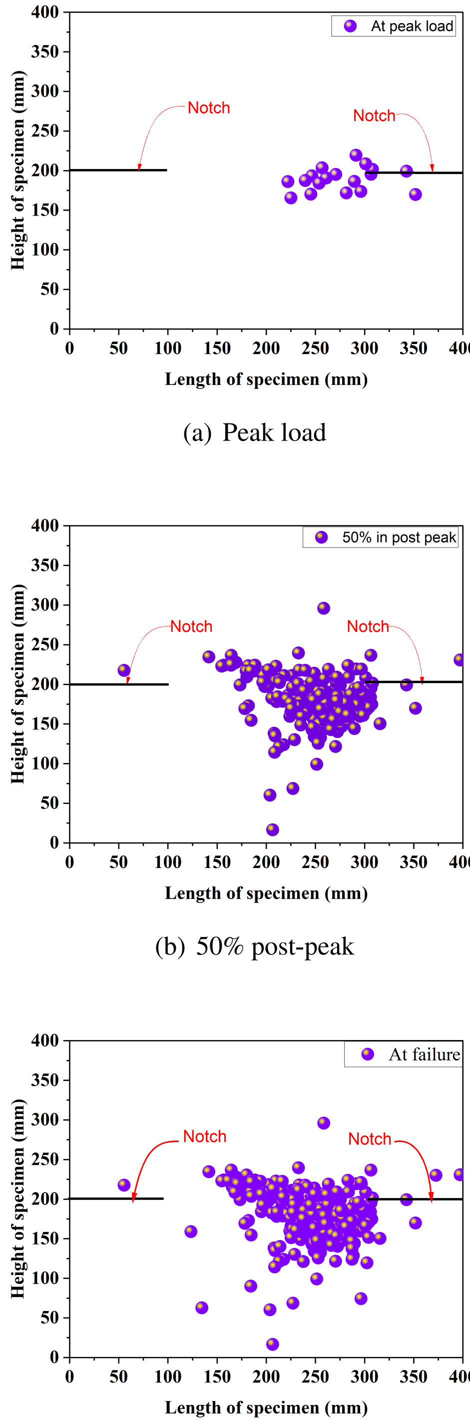

(a) Peak load

(b) 50% post-peak

(c) Failure

Figure 8: Distribution of AE event at different loading percentages (Monotonic loading)

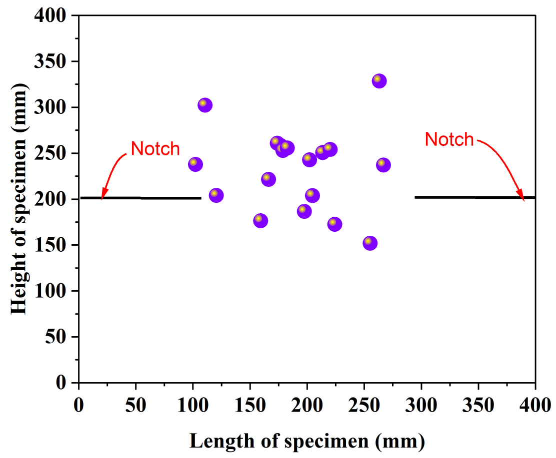

Figure 9: AE events at final cycle (Fatigue loading)

Figure 10 shows the final crack profile obtained from digital image correlation (DIC) using VIC-2D software. The Figures 10(a) and 10(b) depict the strain contours, through which the crack profile is evident for both monotonic and fatigue cases, respectively.

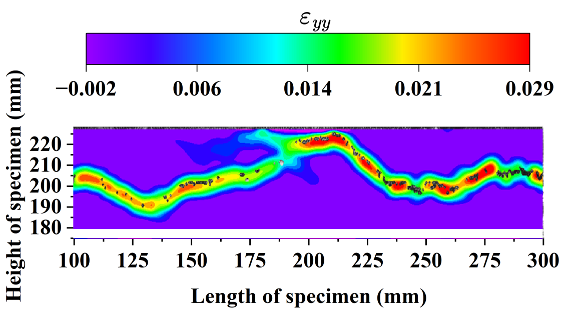

(a) Monotonic loading

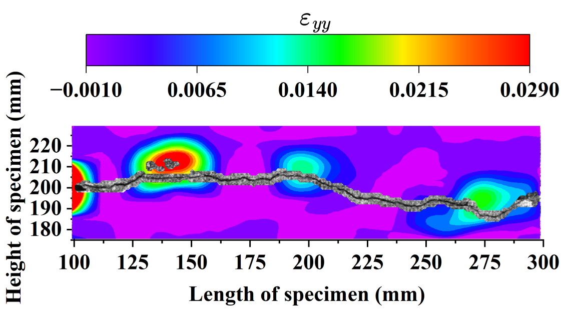

(b) Fatigue loading

Figure 10: Crack profile from DIC

For the DIC, the region of interest (ROI) considered is 50 mm height at the middle portion and 200 mm length measured between left and right notch tips. In the case of monotonic loading, the crack grows continuously during the post-peak softening regime. However, under fatigue loading, the final crack appears suddenly, during the last few cycles of loading.

Figures 11 and 12 show the variation of normalized AE events and normalized cumulative energies, which are plotted against normalized time for monotonic and fatigue loading, respectively. The normalization is done using the corresponding final values. Sharp differences are observed in these figures corresponding to micro-cracks formation under monotonic and fatigue loading. While in the monotonic loading case, there is a continuous formation of micro-cracks, especially in the post-peak softening region, this is not so in the case of fatigue loading. The nucleation of micro-cracks takes place close to the final failure in fatigue loading. The AE energy dissipated as a consequence of micro-crack formation is seen to increase steadily under a monotonic loading case. However, the AE energy in the case of fatigue loading is seen to be dissipated just before the final failure. This behavior indicates that failure under fatigue loading occurs in a brittle manner when compared to monotonic cases, without the formation of a large number of micro-cracks.

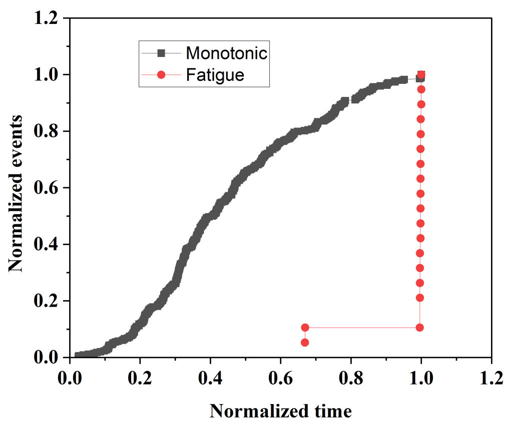

Figure 11: Normalized time versus Cumulative distribution of AE events

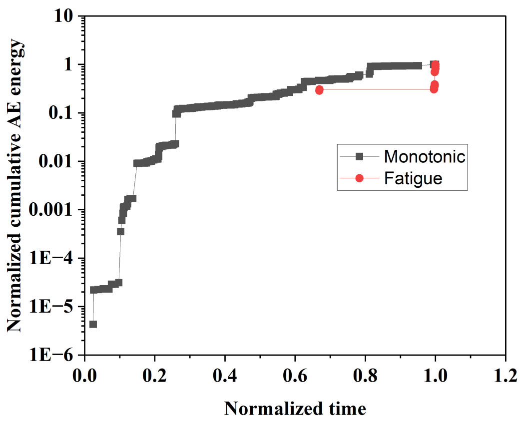

Figure 12: Normalized time variation of cumulative AE energy

The fact that no events are formed during the initial fatigue loading cycles indicates that at lower frequencies, the cracking process does not get triggered. There should be some threshold energy that needs to be supplied to cause micro-cracking under fatigue loading. This needs further attention, and more tests are required to verify the existence of the threshold load limit.

5 Conclusion

In this work, a successful direct tension test was conducted on large-sized double-edge notched concrete prismatic specimens of size 400 x 400 x 100 mm with a notch-to-depth ratio a/d ratio of 0.25 under both monotonic and fatigue loadings. The major conclusions from the obtained results are

- In the monotonically increasing CMOD loading direct tension test, a stable, post-peak softening response was obtained. The micro-cracking process, which was initiated before the peak load, started to grow continuously during the post-peak softening response with the formation of a fracture process zone at one of the notch tips due to fracture localization.

- The tensile strength (f_t) obtained from large-size direct tension test is 4-5% of the compressive strength of concrete, which is much lower than the flexural tensile strength reported in the codes of practice.

- The failure mode under fatigue loading is different from the monotonic counterpart. A relatively brittle mode of failure occurs under fatigue loading without the formation of a large zone of micro-cracks, as seen in the monotonic case.

6 Acknowledgments

The authors thank the Anusandhan National Research Foundation, Government of India, for funding this research through the grant EEQ/2021/000265.

REFERENCES

[1] J. Weerheijm and K. Van Breugel. *Understanding the tensile properties of concrete*. Woodhead Publishing Limited, USA, 2013.

[2] Zdeněk P. Bažant, Jia-Liang Le, and Marco Salviato. *Quasibrittle fracture mechanics and size effect: A first course*. Oxford University Press, Oxford, UK, 2021.

[3] Zdeněk P. Bažant. *Scaling of structural strength*. Elsevier Ltd, Oxford, UK, 2005.

[4] Parvinder Singh, Yogesh R, Sonali Bhowmik, and J.M. Chandra Kishen. Insights into the fracturing process of plain concrete under crack opening. *International Journal of Fracture*, 241:153–170, 2023.

[5] Yogesh R and J.M. Chandra Kishen. Effect of notch size on the fracture behaviour of concrete. In *proceedings of the 11th International Conference on Fracture Mechanics of Concrete and Concrete Structures*, *FraMCoS-11*, Bangalore, India, September 2023. IA-FraMCoS.

[6] Srinithya A, Yogesh R, and J.M. Chandra Kishen. Fatigue fracture behaviour of concrete through wedge-splitting tests.

In *Proceedings of the 11th International Conference on Fracture Mechanics of Concrete and Concrete Structures, (FraMCoS-11)*, Bangalore, India, September 2023. IA-FraMCoS.

[7] J. G.M. Van Mier and M. R.A. Van Vliet. Uniaxial tension test for the determination of fracture parameters of concrete: State of the art. *Engineering Fracture Mechanics*, 69(2):235–247, 2001.

[8] Volker Slowik, Victor E. Saouma, and Andrew Thompson. Large scale direct tension test of concrete. *Cement and Concrete Research*, 26(6):949–954, 1996.

[9] S. K. Lee, S. K. Woof, and Y. C. Song. Softening response properties of plain concrete by large-scale direct tension tests. *Magazine of Concrete Research*, 60(1):33–40, 2008.

[10] Se Jin Choi, Keun Hyeok Yang, Jae Il Sim, and Byong Jeong Choi. Direct tensile strength of lightweight concrete with different specimen depths and aggregate sizes. *Construction and Building Materials*, 63:132–141, 2014.

[11] V. S. Gopalaratnam and Surendra P. Shah. Softening response of plain concrete in direct tension. *Journal of the American Concrete Institute*, 82(3):310–323, 1985.

[12] Alberto Carpinteri. Size effects on tensile fracture properties: a unified explanation based on disorder and fractality of concrete microstructure. *Materials and Structures*, 27:563–571, 1994.

[13] A. Carpinteri and F. Maradei. Three-jack solution to obtain a truly stable and symmetric tensile concrete test. *Experimental Mechanics*, 35(1):19–23, 1995.

[14] Hans W Reinhardt, Hans A W Cornelissen, and Dirk A Hordijk. Tensile tests and failure analysis. *Journal of Structural Engineering*, 112(11):2462–2477, 1987.

[15] H A W Cornelissen, D A Hordijk, and H W Reinhardt. Experimental determination of crack softening characteristics of normalweight and lightweight concrete. *ACI Journal Proceedings*, 59(10):45–56, 1986.

[16] Fatima Zahraa Kachkouch, Camila Carvalho Noberto, Lucas Feitosa de Albuquerque Lima Babadopulos, Abcael Ronald Santos Melo, Amanda Moreira Lima Machado, Nassim Sebaibi, Fouad Boukhelf, and Yassine El Mendili. Fatigue behavior of concrete: A literature review on the main relevant parameters. *Construction and Building Materials*, 338:127510, July 2022.

[17] Bureau of Indian Standards, editor. *Guidelines for concrete mix design proportioning*. Bureau of Indian standards, 1 edition, 2009.

[18] Plain and reinforced concrete - code of practice. In *IS: 456-2000*, pages 1–101. Bureau of Indian standards, New Delhi, 4 edition, 2000.